3D Hierarchical Porous TiO_2 Films from Colloidal Composite Fluidic Deposition

Chiara Dionigi,* Pierpaolo Greco, Giampiero Ruani, Massimiliano Cavallini, Francesco Borgatti, and Fabio Biscarini

Consiglio Nazionale delle Ricerche, Istituto per lo Studio dei Materiali Nanostrutturati, Via P. Gobetti 101, I-40129, Bologna, Italy

Received June 25, 2008. Revised Manuscript Received September 24, 2008

We use a "structure director" colloidal composite to fabricate porous titanium oxide films having a hierarchical pore architecture consisting of mesopores regularly distributed in the macropore shell. The colloidal composite consists of polystyrene beads coated with (ammonium lactate)titanium dihydroxide deposited by means of a fluidic technique. The pore properties and interconnections are controlled at different length scales: a macroscale, which is imposed by the polystyrene beads; a mesoscale, which is controlled by the composition and by the thermal history of the composite; a nanometer-scale, controlled by the nanocrystal sintering in air. Our approach can be extended to a wide class of water-soluble metal oxide precursors; therefore, it opens interesting perspectives for "bottom-up" nanotechnology of functional arrays and devices.

Introduction

The hierarchical organization of a material into a multimodal architecture of pores with controlled size is attractive because it imparts "smart" properties on the structure, in terms of exposed surface, active sites, rheology, and size-selection. This aspect is required for several applications like chromatography, catalysis sensors, photonics, and photovoltaics.[1,2] Interest in the multimodal porosity of titanium oxide, TiO_2, has emerged in the last 10 years because of its optical and electronic properties, which have made it one of the most studied materials in photonic and photovoltaic applications. The control of the porosity in films consisting of TiO_2 inverse opals represents a crucial advance in the field of photonic band gap materials because it leads to a periodic modulation of the refractive index generating a photonic stop band that does not allow the propagation of light with definite frequencies.[3−5]

The substitution of disordered mesoporous TiO_2 films with inverse titania opals, in photovoltaic dye-sensitized solar cells (DSSC)[5−8] represented a breakthrough to improve the conversion efficiency of all solid state DSSC up to the highest limit of 11% obtained by Grätzel et al. in liquid electrolyte based devices.[3,4,8−14] As electron transport strictly depends on the network morphology and interconnection of TiO_2 nanoparticles,[9] attention has been focused on the TiO_2 particle network in order to improve its electron transport and, consequently, to increase the efficiency of DSSCs. Geometric confinement controls the diffusive movement and forces the electron transport to take a specific direction. A one-dimensional network has been considered an excellent compromise to achieve the optimum amount of nanoparticle contacts, generating a direct electron transport. In any case, an inverse opal structure combines the regular spatial arrangement of nanoparticles and an extended specific surface. Two-dimensional geometric confinement in the thin TiO_2 shells can speed up electron transport with respect to a three-dimensional chaotic network, thanks to the reduction of the degrees of freedom for electron movement.[12] Further improvement in the morphology of thin TiO_2 shells indubitably represents an advance in the research on the optimum electron transport network.

Templates made of colloidal crystals of polymeric monodisperse beads have been used to generate TiO_2 inverse opals having differently sized (meso and macro) interconnected pores.[9,15,16] During template removal by thermal treatment,

* Corresponding author. E-mail: c.dionigi@bo.ismn.cnr.it. Tel.: 390516398502. Fax: 390516398540.

(1) Sakatani, Y.; Boissière, C.; Grosso, D.; Nicole, L.; Soler-Illia, G. J. A. A.; Sanchez, C *Chem. Mater.* **2008**, *20*, 1049–1056.
(2) Sanchez, C.; Boissiere, C.; Grosso, D.; Laberty, C.; Nicole, L. *Chem. Mater.* **2008**, *20*, 682–737.
(3) Wong, S.; Kitaev, V.; Ozin, G. A. *J. Am. Chem. Soc.* **2003**, *125*, 15589–15598.
(4) Stein, A.; Li, F.; Denny, N. R. *Chem. Mater.* **2008**, *20*, 649–666.
(5) Somani, P. R.; Dionigi, C.; Murgia, M.; Palles, D.; Nozar, P.; Ruani, G. *Sol Energy Mater. Sol. Cells* **2005**, *87*, 513–519.
(6) Diguna, L. J.; Shen, Q.; Kobayashi, J.; Toyoda, T. *Appl. Phys. Lett.* **2007**, *91*, 023116.
(7) Zhang, Y.; Wang, J.; Zhao, Y.; Zhai, J.; Jiang, L.; Song, Y.; Zhu, D. *J. Mater. Chem.* **2008**, *18*, 2650–2652.
(8) Kuo, C-Y.; Lu, S-Y. *Nanotechnology* **2008**, *19*, 095705.
(9) Grätzel, M. *Nature* **2001**, *414*, 338.
(10) Gates, B.; Park, S. H.; Xia, Y. *Adv. Mater.* **2000**, *12*, 653–556.
(11) Radtchenko, I. L.; Sulkhorukov; G, B.; Gaponik, N.; Kornowski, A.; Rogach, A.m.L.; Möhwald, H. *Adv. Mater.* **200113**, 1684.
(12) Halaoui, L. I.; Abrams, N. M.; Mallouk, T. E. *J. Phys. Chem. B* **2005**, *109*, 6334–6342.
(13) Diguna, L. J.; Murakami, M.; Sato, A.; Kugamai, Y.; Ishihara, T.; Kobayashi, N.; Shen, Q.; Toyoda, T. *Jpn. J. Appl. Phys.* **2006**, *45*, 5563–5568.
(14) Ruani, G.; Ancora, C.; Corticelli, F.; Dionigi, C.; Rossi, C. *Sol. Energy Mater. Sol. Cells* **2008**, *92, 5*, 537–542.
(15) Velikov, K. P.; Christova, C. G.; Dullens, R. P. A.; van Blaaderen, A. *Science* **2002**, *296*, 106–109.
(16) The designation of pores of less than 2 nm, 2 to 50 nm, and over 50 nm size (diameter) as micro-, meso-, and macropores is in accord with accepted IUPAC terminology and definition.

10.1021/cm801734y CCC: $40.75
Published on Web 10/29/2008

random mesoporosity is produced by the partial sintering of oxide nanoparticles in the shells of the macropores.[17]

Controlling mesoporosity in three dimensions represents an innovation for standard templating methods. Specifically for film fabrication, codeposition of ultrafine metal oxide nanoparticles and polymeric templating beads on a substrate was applied to obtain controlled trimodal porosity in SiO_2 films using differently sized templating beads during codeposition.[4,18,19] Up to now, it has only been possible to achieve controlled mesoporosity in TiO_2 films by a templating method based on embossing of the titania sol−gel precursor by a poly-(methyl methacrylate) mold.[20] In both previous examples, the size and shape of the resulting structures are univocally correlated to the size and shape of the template and can not be tuned by varying the process parameters.

In the recent review articles on templating methods,[2,21] the concept of "structure director" was introduced to describe a situation in which the relationship between template morphology and the resulting porous structure is not univocally established but determined by molecule (mainly surfactants) self-assembling.

In this work, we present a colloidal composite acting as a "structure director" for the fabrication of TiO_2 films having controlled and geometrically ordered porosity at different length scales. The composite consists of monodisperse polystyrene beads (PS) coated with a titanium oxide precursor named bis(ammonium lactate)titanium dihydroxide (TALH).[6,13,14,22−24] The multilayered films of ordered TALH/PS composite[10] were deposited in a single step by a fluidic technique called "vertical deposition".[19,25,26] Specifically in these films, annealing [13,27,28] produces an additional controlled porosity at the mesoscale (pore diameter ∼ 30 nm), resulting in a chain morphology that we term "mesochain". Mesochains are confined regions regularly placed in the TiO_2 macropore shells and connected only by poorly accessible porosity caused by the partial sintering of the TiO_2 nanocrystals. We show that a fundamental "structure director" requirement for controlling mesopore distribution in the macropore shells is the absence of reciprocal solubility between the composite components. Highly hydrophilic TALH is orthogonal soluble, at any temperature, to highly hydrophobic polystyrene. By taking advantage of the viscoelastic and relaxation properties of both the polystyrene and the TiO_2 precursor, we developed a process of fabrication leading to a hierarchical pore architecture of the oxide skeleton. In particular, the increase in the Poisson ratio of the TALH coating during the thermal treatment and the critical mass ratio between the PS nanobeads and TALH, which extensively regulates the compliance of the TiO_2 precursor walls, allowed us to select the presence and the characteristic thickness of the mesochains in the metal oxide skeleton. We present results about the fabrication of interpenetrated 3D periodic arrays of differently sized pore shells where 12 mesopores are embedded in the macropore shells.

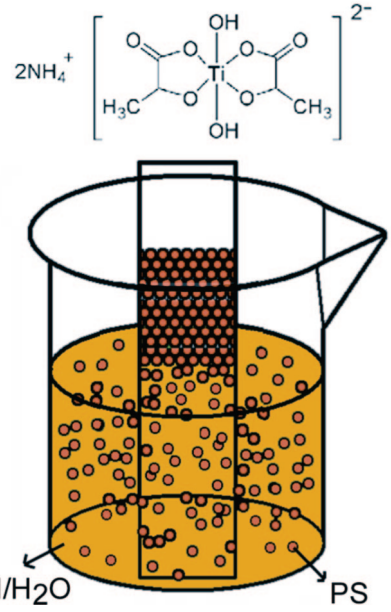

Figure 1. Top, bis(ammonium lactate)titanium dihydroxide (TALH); bottom, vertical deposition process.

The novelty of this work is the demonstration that well-known materials like polystyrene and bis(ammonium lactate)titanium dihydroxide can be properly combined to form a "structure directing" composite that, under annealing, generates periodic and hierarchically ordered meso-macro pore shells in the TiO_2 structures.

Experimental Section

Colloidal Composite Preparation. Bis(ammonium lactate)titanium dihydroxide 50% in water (Aldrich) was used without any further purification (Figure 1). Monodisperse PS, with an average bead size of 340 ± 5 nm, were prepared by surfactant free emulsion polymerization of 3.5 mL of styrene using 0.47 g of ammonium persulfate as radical initiator in 200 mL of deionized water.[29] TALH/PS composite suspension was obtained by mixing 1−20 mg of TALH in 40 mL of deionized water with 17 mg of PS (R = TALH /PS, $0.3 < R < 20$)

Vertical Deposition of TALH/PS Composite on Glass Slides. The vertical deposition method is described elsewhere.[25,26] Vertical depositions on microscope glass slides were performed in closed ambient at 55 °C for 12 h (Figure 1). In ordered composite films, the deposition results extended up to ∼0.5 cm.

(17) Dionigi, C.; Calestani, G.; Ferraroni, T.; Ruani, G.; Liotta, L. F.; Migliori, A.; Nozar, P.; Palles, D. *J. Colloid Interface Sci.* **2005**, *290*, 201–207.
(18) Wang, J.; Li, Q.; Knoll, W.; Jonas, U. *J. Am. Chem. Soc.* **2006**, *128*, 15606–15607.
(19) Meng, Q. B.; Fu, C. H.; Einaga, Y.; Gu, Z. Z.; Fujishima, A.; Sato, O. *Chem. Mater.* **2002**, *14*, 83–88.
(20) Goh, C.; Coakley, K. M.; Mc Gehee, M. D. *Nano Lett.* **2005**, *5*, 1545–1549.
(21) Tiemann, M. *Chem. Mater.* **2008**, *20*, 961–971.
(22) Kim, J.-H.; Fujita, S.; Stiratori, S *Thin Solid Films* **2006**, *499*, 83–89.
(23) Mo Eckel, H.; Giersig, M.; Willig, F. *J. Mater. Chem.* **1999**, *9*, 3051–3056.
(24) Eriksson, J. C.; Ljunggren, S.; Cleasson, P. M. *J. Chem. Soc. Faraday Trans II* **1989**, *85*, 163–176.
(25) Dimitrov, A. S.; Nagayama, K. *Chem. Phys. Lett.* **1995**, *243*, 462–468.
(26) Goldenberg, L. M.; Wagner, J.; Stumpe, J.; Paulke, B. R.; Gornitz, E *Mater. Sci. Eng., C* **2002**, *22*, 405–408.
(27) Dionigi, C.; Stoliar, P.; Porzio, W.; Destri, S.; Cavallini, M.; Bilotti, I.; Brillante, A.; Biscarini, F. *Langmuir* **2007**, *23*, 2030–2036.
(28) Dionigi, C.; Stoliar, P.; Ruani, G.; Quiroga, S. D.; Facchini, M.; Biscarini, F. J. *Mater. Chem.* **2007**, *17*, 3681–3686.
(29) Dionigi, C.; Nozar, P.; Di Domenico, D.; Calestani, G. *J. Colloid Interface Sci.* **2004**, *275*, 445–449.

Thermal Treatments. Dry samples were thermally processed in air up to 450 °C with a thermal ramp of 3 °C/min followed by a 2 h stationary step at 450 °C.

Thermal and Calorimetric Analysis. Differential scanning calorimetry analysis (DSC) was performed with a STA1500 System (Simultaneous Thermal Analyzer) in an air atmosphere. A temperature ramp of 5 °C/min was used.

Raman Measurements. Raman spectra were collected in back scattering geometry using a Renishaw 1000 micro-Raman instrument equipped with charge coupled device CCD cameras and microscope lense with 50× magnification. The excitation was provided by the 632.8 nm line of a HeNe laser. Because the cutoff edge of the holographic filter does not allow sharp detection of the E_g Raman mode of TiO_2 around 145 cm^{-1}, Raman spectra were also collected using a FT-Raman RFS100 Bruker system equipped with a liquid nitrogen cooled Ge detector, an Nd:YAG laser line at 1064 nm was used as an excitation source. In both cases the resolution was 1.0 cm^{-1} and the accuracy better than 0.5 cm^{-1}.

Scanning Electron Microscopy. The morphology of the inverse structures of the titanium oxide samples were detected by scanning electron microscopy (SEM). SEM analyses of bead and titanium oxide structures were performed using a Philips XL30 electron microscope operating at 30 kV accelerating voltage. The samples were metallized by sputtering a 3−5 nm thick layer of gold on the surface.

Atomic Force Microscopy. Atomic force microscopy (AFM) images were recorded with a stand alone AFM (SMENA NT-MDT Moscow) operating in air, in intermittent contact mode (25 °C with relative humidity 55%). Silicon cantilever (NT-MDT NSG10, with a typical curvature radius of 10 nm tip and a typical resonant frequency 255 KHz) were used. All images are unfiltered. The topographic images were corrected line-by-line for background trend effects by removal of the second-order polynomial fitting.

Results and Discussion

A crucial point in the mesochain formation is the thermal treatment of TALH/PS films. We characterized thermally the TALH/PS composites and followed TiO_2 skeleton formation by Raman spectroscopy. Scanning electron microscopy (SEM) and atomic force microscopy (AFM) were used to measure pore size and to detect morphology transformation caused by TALH/PS composition and by annealing temperature.

The thermal behavior of the composite during annealing was followed by differential scanning calorimetric analysis (DSC). The resulting DSC curve is reported in Figure 2. Polystyrene thermal processes in air include glass transition (∼93 °C), melting (240 °C) and combustion (400−450 °C).[17] From DSC in air of TALH/PS composite it turns out that polystyrene burns at 412 °C. On the other hand, TALH undergoes several endothermic processes in the range 148−240 °C eliminating NH_3 and CO_2 groups, as emphasized in Figure 2a, and exothermic reactions in the range 280−320 °C, maybe due to the combustion of organic ligands. The effects on sample morphology after TALH endothermic reactions was demonstrated by annealing a set of composite samples at 240 °C and, in turn, rinsing them in tetrahydrofuran (THF) to remove PS. TALH that has been thermally modified at $T \approx 240$ °C will be called MTALH. SEM micrograph of a MTALH sample after the solvent washing is shown in Figure 2b. It is evident that thermal treatment at 240 °C is sufficient to modify TALH into a periodic skeleton that remain self-standing after PS removal by solvent.

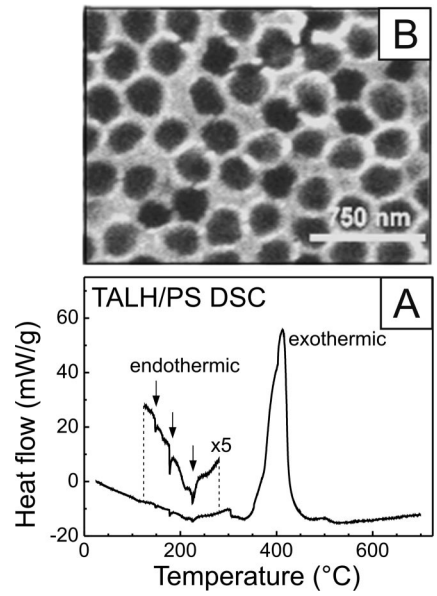

Figure 2. (a) Differential scanning calorimetric analysis of a TALH/PS composite: endothermic reactions are reported in a 5× scale; (b) SEM micrograph of $R = 2.4$ sample after annealing at 240 °C (MTALH) followed by PS removal by tetrahydrofuran.

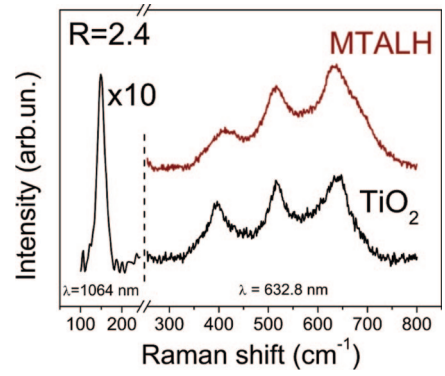

Figure 3. RAMAN spectra of $R = 2.4$ samples. The red line refers to the MTALH sample after PS removal by THF; the black line refers to the TiO_2 sample after 450 °C thermal treatments.

MTALH samples rinsed in THF were analyzed by Raman spectroscopy at $\lambda = 632.8$ and 1064 nm. We found that crystalline TiO_2 nanoparticles (anatase phase), smaller than 3 nm, had already formed at 240 °C in air (Figure 3, red line)[17,30] The organic TALH residuals in MTALH samples caused an intense luminescence background, exciting at $\lambda = 632.8$ nm. Exciting at $\lambda = 1064$ nm, it was not possible to detect any Raman signal because of the excessive luminescence. The luminescence background almost disappeared at both excitations only after a thermal ramp to 450 °C in air that removed all organics and transformed TALH into the TiO_2 anatase phase (Figure 3, black line). Moreover, nanocrystals size increased up to 7 nm because of TiO_2 nanocrystal sintering.[17]

(30) Kelly, S.; Pollak, F. H.; Tomkiewicz, M. *J. Phys.Chem. B* **1997**, *101*, 2730–2734.

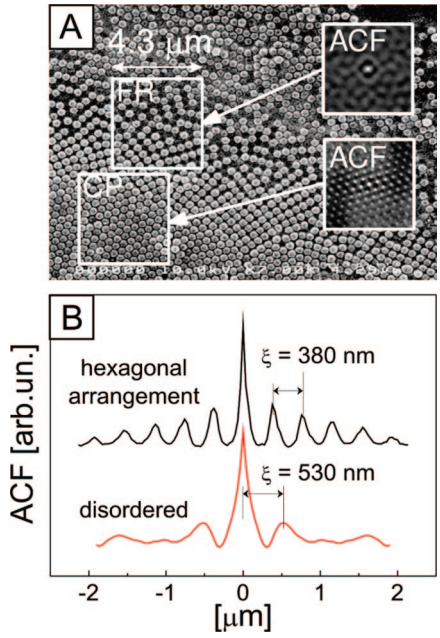

Figure 4. (a) SEM image of close packing dynamics, as revealed by nanosphere arrangement during the vertical deposition of TALH/PS, (b) Profiles extracted from 2D autocorrelation maps (ACF) plotted in the inset of two details representing the fractal (FR) and hexagonal close packed (CP) configurations of the spheres' array.

The production of nanostructured TiO_2 film via TALH/PS composite deposition is based on the coating capability of TALH on PS.[13] We followed the dependence of the final TiO_2 nanostructures on PS coating by TALH that increased until PS surface saturation by varying in the suspension used for the vertical deposition the mass ratio TALH/PS (R) and keeping PS mass, PS diameter, deposition temperature, and water volume constant.[19,25] During the vertical deposition procedure the component concentrations are not constant during film growth, we considered only films deposited at 12 h, assuming that, in these hours, the concentrations are only slightly modified. The progressive close-packing of the nanospheres during vertical deposition is shown in Figure 4, where the dynamics of the film's growth was captured by the SEM image. The polystyrene nanospheres arrangement starts from disordered assemblies and goes through fractal formation toward the maximum hexagonal close packing. The appearance of this configuration is related to the fact that a correct ratio between PS nanospheres and titanium dioxide precursor is reached by liquid phase evaporation. The ordered part of the film was easily recognized by sight since TALH/PS film gave opal-like red reflections. Confirmation of the importance of the TALH concentration for ordering is given in Figure 4b where the pair correlation function (PCF) is given for samples with a different ratio *R*. Using the description given for hard sphere processes[31] (see the Supporting Information), we saw ordered clustering of PS spheres only within small windows of analysis, whereas there was no sound evidence of a long correlation length in the full SEM image, because of various patches present in the outer layer.

(31) Mecke J.; Stoyan, D.; Kendall, W., Eds.; *S. Stochastic Geometry and Its Applications*, 2nd ed.; John Wiley: New York, 1995.

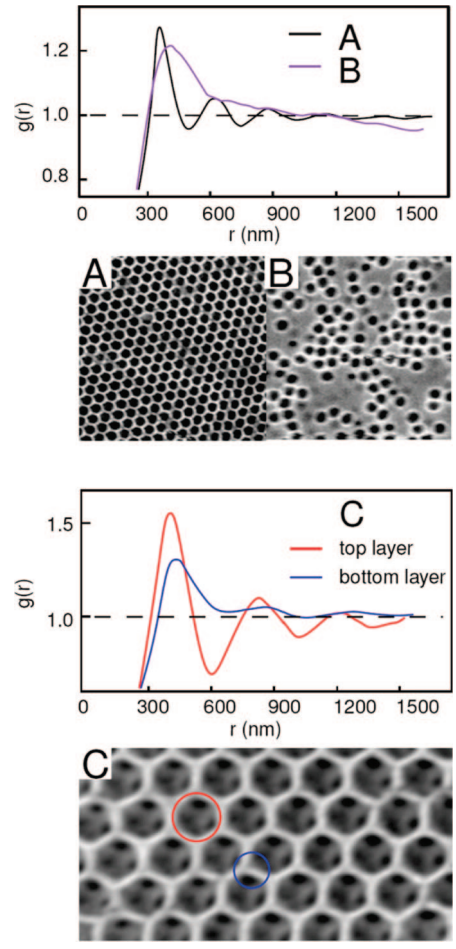

Figure 5. Pair correlation function ($g(r)$) for pattern obtained in condition of optimal ratio ($R = 3.5$) between nanospheres and titanium dioxide precursor (A), and at higher concentration of precursor ($R = 12$). In (C), the pair correlation function is calculated among the positions of resulting macropores in the inverse structure. The persisting correlation in the 3D structure is evaluated for two superimposed layers directly from the SEM image.

TALH/PS films transformed into TiO_2 anatase films after annealing at 450 °C showed well-ordered arrays of macropores whose size was estimated to bee <30% of the PS size by SEM microphotograph.

We observed that R strongly influenced macropore array and macropore size. The optimum macropore array was achieved at $R = 3.5$ as confirmed by PCF calculated from the corresponding SEM images as shown in Figure 5, where a comparison with a sample obtained from $R \approx 12$ is given. This value of *R* is almost at the limit for ordered macropore array generation. The correlation on sample $R = 3.5$ reveals a characteristic frequency in ordered arrays at ~350 nm. However, the distance between cavities, also at higher *R*, can not be less than 300 nm, giving more evidence of the fact that adsorption of TALH is confined on the sphere surface. The order conveyed in the 3D structure can be studied for two superimposed layers directly from the sem image (see Figure 5b). The holes resulting from macropore interconnections were not visible for all the samples in the SEM micrographs. Anyway, it was possible to pursue this specific analysis for the optimal ratio between PS and TALH. The coordinates of the characteristic holes left by spheres interconnections have been analyzed with the same algorithm

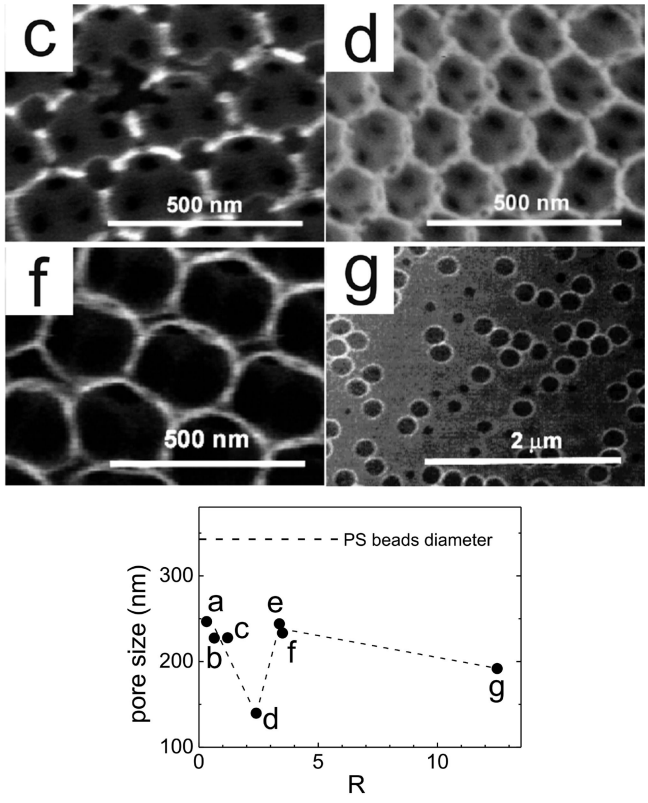

Figure 6. Pore size of TiO_2 samples after annealing at 450 °C, coming from different TALH/PS ratios (R). The dotted line represents the diameter of the original PS. The dotted red line highlights the "discontinuity" point in pore diameter. SEM micrographs of the most significant samples are marked with the corresponding letters of the graph.

given for correlation between the main cavities in the inverse opal, and a characteristic frequency of ~380 nm can be established from PCF peak analysis, both for the first and second layer of the oxide structure.

The pore size trend was collected by varying R (Figure 6). The minimum pore size was observed at $R = 2.4$. This value corresponded to an evident discontinuity of the trend. In this case, hexagonal macropore array was conserved and resulted in being regularly bordered by "large mesopores" (~30 nm). These mesopores seem to be regularly concatenated into each single shell. They have a chain appearance that we call "mesochain" morphology.

An explanation of the mesochain morphology is proposed in Figure 7. As TALH/PS samples achieved 240 °C, TALH coating, decomposed into TiO_2 nanocrystals, mainly expelling the most hydrophilic groups (NH_3, CO_2) of TALH. We assume that in the range 240−400 °C (after polystyrene MP and before polystyrene combustion), liquid polystyrene infilled in the hydrophobic MTALH coating consisting of TiO_2 nanocrystals, amorphous TiO_2, and organic residuals. In particular, liquid polystyrene flowed trough the MTALH and was forced to deposit at the original PS junctions by lateral capillary forces.[32] We assume that polystyrene streams were regulated by TiO_2 nanocrystal sintering and their concentration in the MTALH coatings. MTALH coating by $R = 2.4$ was able to trap liquid polystyrene in sorts of "mesoreservoirs", immersed in the MTALH coating, and

(32) Kralchevsky, P.; Nagayama, K. *Langmuir* **1994**, *10*, 23–36, 23.

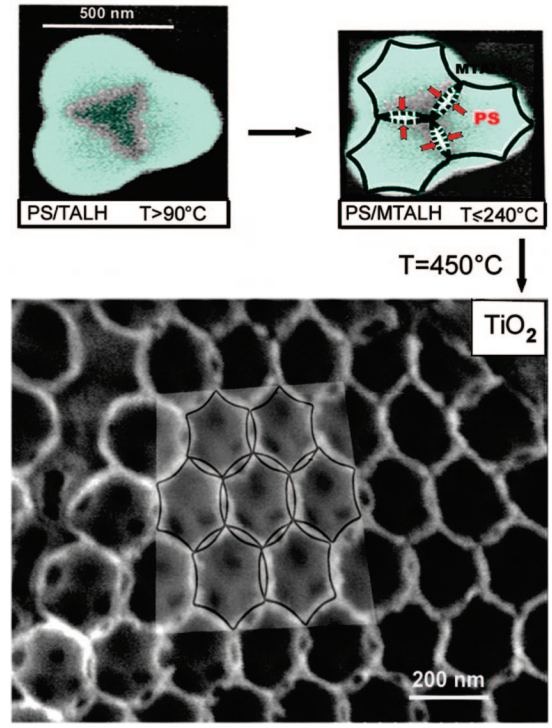

Figure 7. Mechanism for the nanochain morphology of $R = 2.4$ samples. It is presented as a SEM micrograph of PS/TALH composite self-assembled on glass substrate at $T > 90$ °C; a model of polystyrene infiltration trough the MTALH coating at 240 °C and consequent meso-reservoir formations; (3) the resulting mesochain morphology after annealing at 450 °C.

regularly placed at the original PS junctions. Because the mesoreservoirs subtract polystyrene from melted PS, the TiO_2 inverse structure, reproduced smaller templating beads, thus determining the decrease in the macropore size. It is significant that some peculiarities also appeared in samples obtained from $R = 3.5$ as shown in the micrograph reported in Figure 6f. In these samples, the regular macropore shells are transformed into TiO_2 bundles bordering the macropores.

The surfaces of THF-treated MTALH and thermal treated TiO_2 samples were compared by AFM operating in non contact mode. We specifically investigated samples obtained from $R = 2.4$. Well-ordered shells made of MTALH are shown. MTALH shells, even after THF washing, seem to be highly dense, maybe because of residual polystyrene. The morphology of THF-treated MTALH is described by a regular distribution of macro pores spatially organized but non-well-ordered. Thermally treated samples appear more ordered and regular with respect to the MTALH sample, as shown in Figure 8a. Macropore shrinkage after the combustion of organic residuals in MTALH is evident when MTALH is compared with TiO_2 films (Figure 8b).

On the other hand, after thermal treatment at 450 °C in an air atmosphere, in the AFM images, the resulting TiO_2 sample results perfectly organized in a close packing structure with a macropore size of about 125 ± 7 nm (Figure 8b), according to the SEM measurements. Furthermore the TiO_2 nanostructures which form in the places of the original PS junctions form an ordered distribution of nanoclusters whose apparent diameter is ~25 nm (because of the tip deconvolution, all the smaller structures always appear to have 20 nm width).

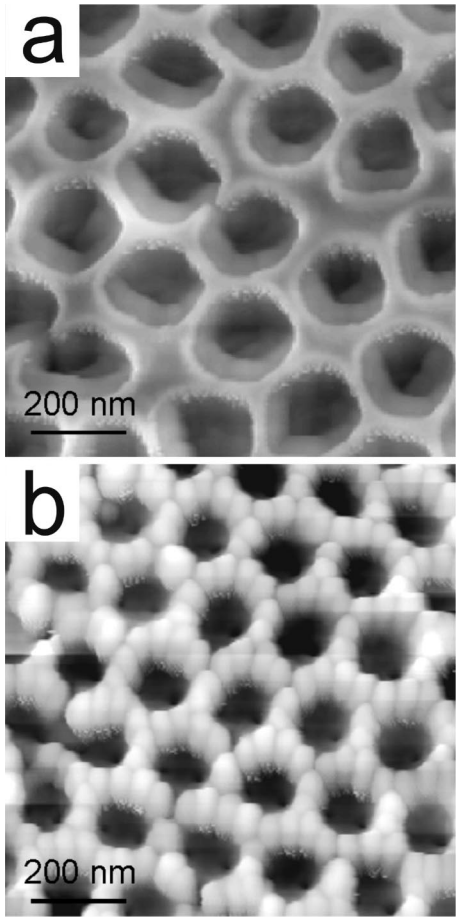

Figure 8. AFM operating in non contact mode of the surfaces of a $R = 2.4$ sample in (a) the MTALH form after THF washing and (b) thermal-treated TiO_2 sample.

Conclusions

We have shown that PS/TALH colloidal composite can be deposited by a simple fluidic method on a glass substrate. The composite acts as a "structure director" to fabricate 3D nanostructured films of anatase TiO_2 with hierarchical pore distribution and an unusual meso-chain morphology. We found that the regular distribution of "large mesopores" strictly depends on a specific composition (TALH/PS ratio = 2.4) of the starting colloidal composite in water. Ordered mesopores are obtained with high reproducibility and they depend on physical characteristics (MP, burning temperature) of both the monodisperse beads (PS) and the TiO_2 precursor (TALH). Under annealing, the resulting nanostructured TALH/PS composite undergoes several transformations until the TiO_2 skeleton "freezes" the morphology induced by thermal treatments.

We believe that the bimodal porous architecture can be potentially transformed into a bimodal periodic distribution of active materials (i.e., dyes, conductive polymers, nanoparticles, drugs) incrorporated into the TiO_2 skeleton for applications in sensing,[33] photocatalysis,[34,35] and photovoltaic thecnology.[5−8] A further perspective of our method could be the integration with unconventional lithographies [36,37] that can allow the microstructuration of the colloidal composite precursor.

Acknowledgment. M.C. is supported ESF-EURYI -DYMOT. We acknowledge Dr. Pablo Stoliar and Dr. Alessandra Sutti for scanning electron microscopy images.

Supporting Information Available: Additional information. This material is available free of charge via the Internet at http://pubs.acs.org.

CM801734Y

(33) Sutti, A.; Baratto, C.; Calestani, G.; Dionigi, C.; Ferroni, M.; Faglia, G.; Sberveglieri, G. *Sens. Actuators, B* **2008**, *130*, 567–573, 1.
(34) Chen, J. I. L.; von Freymann, G.; Kitaev, V.; Ozin, G. A. *J. Am. Chem. Soc.* **2007**, *129*, 1196–1202.
(35) Camera-Roda, G.; Santarelli, F.; Martin, C. *Solar Energy* **2005**, *79*, 343–352.
(36) Cavallini, M.; Murgia, M.; Biscarini, F *Nano Lett.* **2001**, *1*, 193–195.
(37) Cavallini, M.; Stoliar, P.; Moulin, J. F.; Surin, M.; Leclere, P.; Lazzaroni, R.; Breiby, D. W.; reasen, J. W.; Nielsen, M. M.; Sonar, P.; Grimsdale, A. C.; Mü llen, K.; Biscarini, F. *Nano Lett.* **2005**, *5*, 2422.